Journal of Electrical Engineering & Technology
https://doi.org/10.1007/s42835-025-02453-6

ORIGINAL ARTICLE

Doppler Resolution Enhancement Algorithm Based on Extrapolation for FMCW Radar

Youngdoo Choi[3] · Seonghyun Jang[4] · Bong-seok Kim[1] · Sangdong Kim[1,2]

Received: 29 April 2025 / Revised: 4 September 2025 / Accepted: 10 September 2025

Abstract
This paper proposes a Doppler resolution enhancement algorithm based on signal extrapolation for frequency-modulated continuous wave (FMCW) radar systems. In conventional FMCW radar, Doppler estimation is performed by repeatedly transmitting multiple chirp signals and analyzing the phase variations of the received signals via the fast Fourier transform (FFT). However, when multiple targets have similar velocities, their Doppler shifts become indistinguishable, often resulting in the detection of multiple targets as a single peak in the Doppler spectrum. A common approach to resolving this issue is to increase the observation time, which improves resolution but at the cost of additional resources. To overcome this limitation, the proposed method enhances Doppler resolution without extending the observation window by extrapolating the received signal through simple signal manipulations. Simulation results verify that the proposed algorithm achieves improved Doppler resolution without incurring additional resource overhead. Compared to the conventional FFT approach, it achieves up to 33% reduction in RMSE and up to 68% reduction in missing rate under moderate SNR and closely spaced targets, while maintaining a similarly low computational cost.

Keywords FMCW radar · Doppler · FFT · Resolution improvement · Low complexity

1 Introduction

Radar sensors have become an integral part of modern sensing systems, playing a central role in various applications such as automotive safety, industrial automation, surveillance, aerospace, and biomedical monitoring. Since they are robust even in harsh environmental conditions such as rain, fog, darkness, and dust, they are generally more advantageous than optical or infrared sensors that rely on favorable lighting and viewing angles [1, 2]. Radar systems can penetrate obstacles and operate in scenarios other than viewing angles, enabling reliable object detection and tracking even in chaotic or dynamic environments.

The growing interest in autonomous driving, intelligent transportation systems, and robotics has further accelerated the need for radar systems that are not only reliable but also compact and cost-effective. Frequency-modulated continuous-wave (FMCW) radar has emerged as a prominent solution due to its ability to simultaneously estimate range and velocity with relatively low hardware complexity [3–5]. Unlike ultra-wideband or impulse radars, FMCW radars achieve high range resolution while requiring lower ADC sampling rates by reducing power consumption and

Co-corresponding Author: Sangdong Kim.

✉ Bong-seok Kim
remnant@dgist.ac.kr

✉ Sangdong Kim
kimsd728@dgist.ac.kr

Youngdoo Choi
chododo78@navy.ac.kr

Seonghyun Jang
jang.sh@keti.re.kr

1 Division of Future Mobility Technology, DGIST, Daegu, Korea

2 Division of Future Mobility Technology, School of Interdisciplinary Studies, DGIST, Daegu, Korea

3 Electronics and Control Engineering, ROK Navy Academy, Changwon-si, Korea

4 Mobility Platform Research Center, Korea Electronics Technology Institute, Seongnam-si, Korea

Published online: 26 September 2025

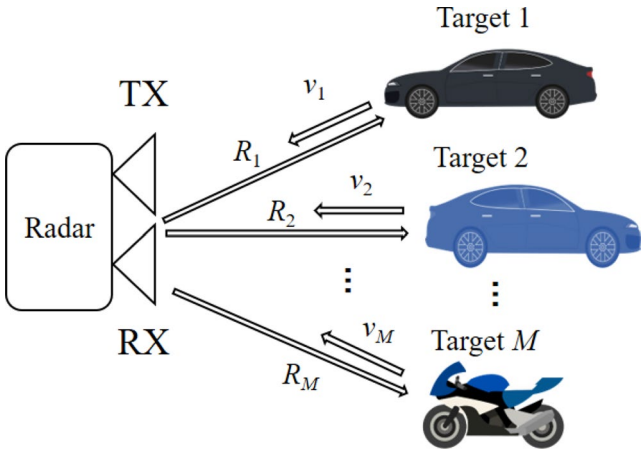

Fig. 1 System model

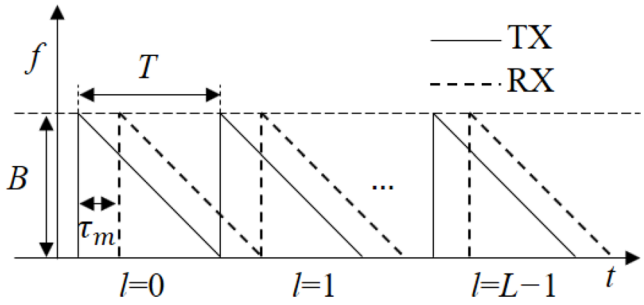

Fig. 2 Structure of TX and RX signals of FMCW radar

cost. Furthermore, unlike continuous-wave (CW) radar systems, FMCW radar enables both range and Doppler measurements from a single transmission, making it suitable for high-mobility and time-critical applications.

In FMCW radar, the fast Fourier transform (FFT) is widely used for both range and Doppler estimation due to its computational efficiency and simplicity [6]. The introduction of the FFT algorithm significantly reduced the processing time required to analyze frequency-domain signals [7]. However, FFT-based methods are fundamentally limited by their resolution, which is governed by the time-bandwidth product. When multiple targets exhibit similar velocities, their Doppler frequencies can fall within the same FFT bin, making them indistinguishable in the frequency domain [8].

In [9], an extrapolation-based method for FMCW radar was proposed to improve resolution using beat-frequency slices in the short time Fourier transform (STFT) domain. The technique involves extrapolating frequency-domain slices between sweeps, followed by phase correction and inverse STFT reconstruction. This approach effectively extends the usable observation window but incurs increased computational complexity due to time-frequency transforms and prediction-based filtering.

To address these limitations, super-resolution techniques such as the Estimation of Signal Parameters via Rotational Invariance Techniques (ESPRIT) and the Multiple Signal Classification (MUSIC) algorithm have been proposed [10–13]. These algorithms exploit the signal subspace to resolve closely spaced spectral components beyond the classical resolution limit.

Nevertheless, such methods are computationally intensive and often require prior knowledge of the number of sources, which may not be available in practical real-time radar systems. Various alternative techniques have been explored to improve resolution without high computational cost. For example, signal extrapolation and virtual opening expansion were used to improve resolution synthetically [8].

In this paper, we propose a novel Doppler resolution enhancement algorithm that does not require additional resources or complex subspace estimation. The proposed algorithm enhances Doppler resolution by extrapolating the chirp signal through simple mathematical operations, thereby extending the effective observation window without increasing resource usage. Furthermore, mathematical analysis demonstrates that interference terms are not dominant even in multi-target scenarios. Through simulation results and complexity analysis, we show that the proposed approach provides improved performance in resolving closely spaced Doppler components compared to conventional FFT-based techniques.

The remainder of this paper is organized as follows. Section 2 and Sect. 3 describe the FMCW radar signal model and Doppler estimation algorithms as related work. Section 4 presents the proposed algorithm in detail, including its mathematical formulation. Section 5 provides simulation results and computation complexity. Section 6 concludes the paper and discusses future work.

2 System Models

This section discusses the system model of radar signals. Among various radar types, the FMCW radar system is considered. Figure 1 illustrates the system model under consideration. A total of MMM targets are assumed, where the m-th target is located at a distance R_m from the radar and is moving at a velocity v_m.

Figure 2 illustrates the structure of the transmitted and received signals in an FMCW radar system. A total of L symbols are transmitted and received per frame. In Fig. 2, B represents the bandwidth, T denotes the duration of a chirp symbol, and τ_m indicates the delay component caused by the m-th target, which is determined by the distance R_m.

The beat signal corresponding to the l-th chirp in an FMCW radar system can be expressed as follows:

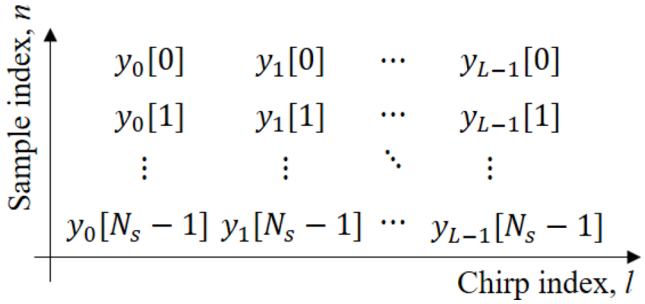

Fig. 3 Data structure of beat signal according to sample index and chirp index

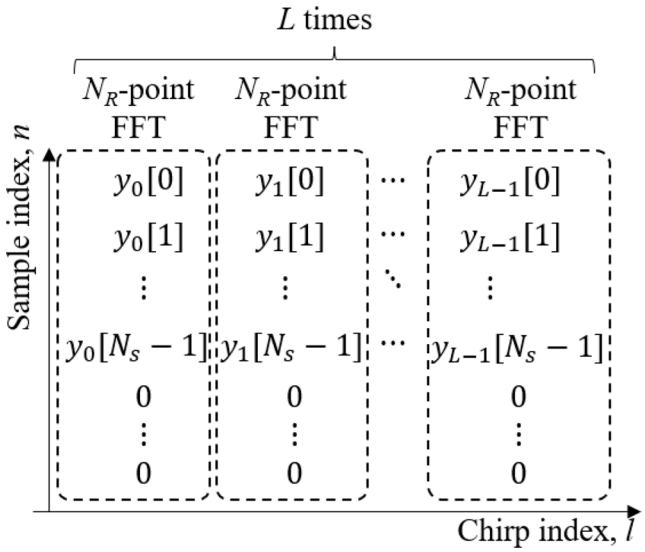

Fig. 4 Structure of range estimation of the conventional FFT-based algorithm

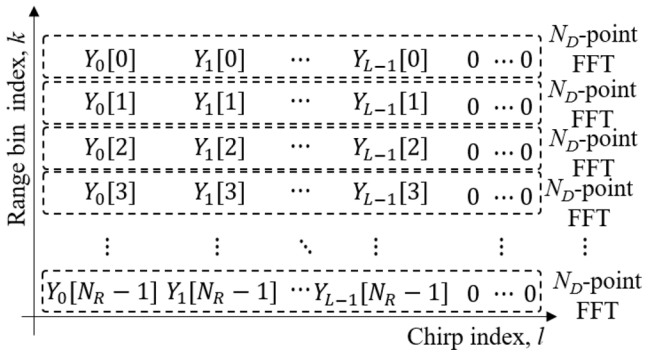

Fig. 5 Structure of Doppler estimation of the conventional FFT-based algorithm

$$y_l(t) = \sum_{m=1}^{M} a_m \underbrace{\exp(j2\pi\mu_m t)}_{\text{range term}} \underbrace{\exp(j2\pi f_m^D Tl)}_{\text{velocity term}} + z_l(t) \quad \text{for } 0 \leqslant l \leqslant L-1 \tag{1}$$

where a_m is the complex coefficient that includes the amplitude and phase components of the signal reflected by the m-th target, μ_m is the slope of the FMCW radar, f_m^{D} represents the Doppler frequency caused by the velocity v_m of the target, and $z_l(t)$ denotes additive complex Gaussian noise. The beat signal $y_l(t)$ is sampled using ADC with a sampling interval t_s, and the resulting discrete digital signals is expressed as:

$$y_l[n] = \sum_{m=1}^{M} a_m \exp(j2\pi\mu_m n t_s) \exp(j2\pi f_m^D Tl) + z_l[n]. \tag{2}$$

Figure 3 shows the data structure based on (2). The vertical axis represents the sample domain n, while the horizontal axis corresponds to the chirp domain l. By estimating the frequency in the vertical direction, i.e., μ_m, the range R_m can be determined. Similarly, by estimating the frequency in the horizontal direction, the Doppler frequency f_m^{D} can be obtained, enabling the estimation of the target's velocity.

3 Range and Doppler Estimation Algorithms Based on FFT

3.1 Conventional FFT-Based Algorithm

In this section, the algorithm for estimating range and Doppler by performing FFT on the beat signal is described. First, an N_R-point FFT is performed where N_R is the FFT size used for range estimation, and it is larger than the number of samples N_s, as shown in Fig. 4. Additionally, zero-padding is applied to make the FFT input length equal to N_R, which is denoted as $y_l^o[n]$, i.e., $y_l^o[n] = [y_l[0], ..., y_l[N_S-1], 0, ..., 0]^{\mathrm{T}}$ where $(\cdot)^{\mathrm{T}}$ is transpose operator. Specifically, the k-th FFT output for $y_l^o[n]$ is denoted by $Y_l[k]$ and is expressed as follows [14]:

$$\mathrm{Y}_l[k] = \sum_{n=0}^{N_R-1} y_l^o[n] \exp\left(-\frac{j2\pi kn}{N_R}\right), \text{ for } 0 \leqslant k \leqslant N_R - 1. \tag{3}$$

Then, N_R times N_D-point FFT is performed on range FFT output $Y_l[k]$ in order to estimate Doppler as shown in Fig. 5. The q-th FFT output for Doppler estimation $\tilde{Y}_q[k]$ is expressed as follows:

$$\tilde{Y}_q[k] = \sum_{l=0}^{N_D-1} Y_l^o[k] \exp\left(-\frac{j2\pi ql}{N_D}\right), \text{ for } 0 \leqslant q \leqslant N_D - 1 \tag{4}$$

where $Y_l^o[k]$ is the zero-padded version of $Y_l[k]$, i.e., $Y_l^o[k] = [Y_0[k], ..., Y_{L-1}[k], 0, ..., 0]$ of length L, obtained by appending N_D–L zeros in order to perform N_D-point FFT.

Subsequently, the final range and velocity of the target are estimated through the FFT output $\tilde{Y}_q[k]$ processed using a constant false alarm rate (CFAR) algorithm. Then, using

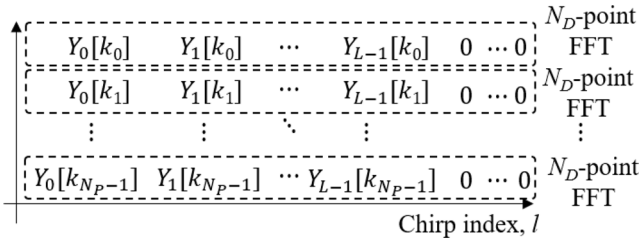

Fig. 6 Structure of Doppler estimation of the RoI based algorithm

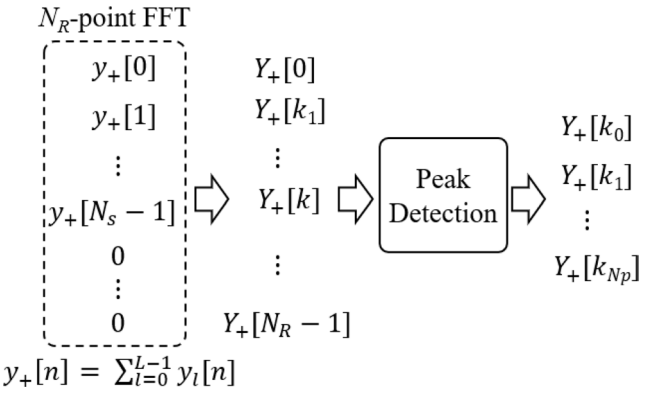

Fig. 7 Structure of RoI detection algorithm

the m-th estimated range bin index $\hat{k}_m$ and Doppler index $\hat{q}_m$, i.e., the ordered pairs $(\hat{k}_m,\hat{q}_m)$ for $m=1, 2,\ldots, M$, the estimated range $\hat{R}_m$ and velocity $\hat{V}_m$ are calculated as follows [15]:

$$\hat{R}_m = \frac{c_0 \hat{k} f_s}{2\mu N_R} \tag{5}$$

$$\hat{V}_m = \frac{c_0 \hat{q}_m}{2 f_c T N_D} \tag{6}$$

where c_0 is the velocity of electromagnetic, i.e., $c_0=3\times10^8$ m/s.

3.2 RoI-Based Complexity Reduction FFT-Based Range and Velocity Estimation Algorithm

This section describes a complexity-reduced FFT-based range and velocity estimation algorithm utilizing a region of interest (RoI), referred to hereafter as the RoI-based algorithm. In the conventional algorithm discussed in Sect. 3.1, an N_R–point range FFT is applied to each of the L chirps, resulting in N_R chirp domain signals of length L. Then, N_D–point Doppler FFT is performed on each of these N_R signals. In contrast, as shown in Fig. 6, the RoI-based algorithm reduces computational complexity by restricting Doppler estimation to N_P selected range bins, which are identified as likely to containing targets, instead of processing all N_R signals where N_P is the number of the detected peaks.

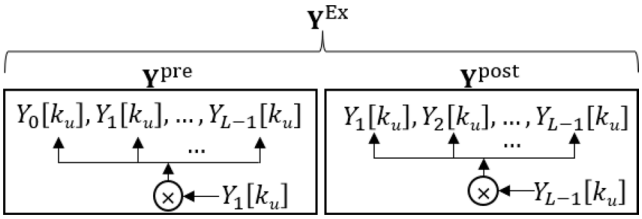

Fig. 8 Structure of the proposed extrapolation algorithm

To aid understanding, Fig. 7 illustrates an example of RoI detection. In Fig. 7, all chirp signals are summed to improve SNR [14]. The summed signal $y_+[n]$ is processed by an N_R -point FFT, followed by peak detection. As a result of the RoI detection process, N_P indices are identified, i.e., k_u for $u=0, 1, \ldots, N_P-1$, representing the range bins estimated to contain targets.

Subsequently, N_P times N_D–point FFT for Doppler estimation is performed only for for $0\le u\le N_P-1$ instead of $0\le k\le N_R-1$ as in the conventional algorithm. The u-th FFT output of the RoI based algorithm is denoted by $\tilde{Y}_q^{\mathrm{RoI}}[u]$ and is expressed as follows:

$$\tilde{Y}_q^{\mathrm{RoI}}[u] = \sum_{l=0}^{N_D-1} Y_l^o[k_u] \exp\left(-\frac{j2\pi ql}{N_D}\right), \text{ for } 0 \leqslant q \leqslant N_D-1 \tag{7}$$

where $Y_l^o[k_u]$ is the zero-padded version of $Y_l[k_u]$, i.e., $Y_l^o[k_u] = Y_l[k_u]$ for $0 \leqslant u \leqslant N_P-1$ and $Y_l^o[k_u] = 0$ for $N_P\le u\le N_D-1$. Since N_R is typically much larger than N_P, the computational complexity is significantly reduced.

4 Proposed Range and Doppler Estimation Algorithm

4.1 Proposed Extrapolation Algorithm

This section describes an FFT-based estimation algorithm with improved resolution, achieved through simple signal processing. The process up to the Doppler FFT estimation is identical to the RoI-based algorithm described in Sect. 3.2. In other words, the proposed extrapolation algorithm is applied to the component $Y_l[k_u]$, which corresponds to the k_u-th row among the $N_P\times L$ range bins estimated to contain targets through the RoI detection process.

After RoI detection, the selected signal corresponds to the k_u-th range bin; that is, $Y_l[k_u]$ is used for the proposed extrapolation. Figure 8 illustrates the proposed extrapolation algorithm. In the proposed algorithm, the extrapolated vector is denoted by $\mathbf{Y}^{\mathrm{Ex}}$, which is constructed by concatenating two vectors, $\mathbf{Y}^{\mathrm{pre}}$ and $\mathbf{Y}^{\mathrm{post}}$, both of which are generated based on $Y_l[k_u]$, i.e., $\mathbf{Y}^{\mathrm{Ex}} = [\mathbf{Y}^{\mathrm{pre}}\ \mathbf{Y}^{\mathrm{post}}]$. The front vector of length L is denoted by $\mathbf{Y}^{\mathrm{pre}}$ and expressed as:

$$\begin{aligned}\mathbf{Y}^{\mathrm{pre}} &= \left[Y_0^{\mathrm{pre}}[k_u],\, Y_1^{\mathrm{pre}}[k_u], ..., Y_{L-1}^{\mathrm{pre}}[k_u]\right] \\ &= Y_1[k_u] \times \left[Y_0[k_u],\, Y_1[k_u], ..., Y_{L-1}[k_u]\right],\end{aligned} \tag{8}$$

where $Y_l^{\mathrm{pre}}[k_u]$ is the l-th element of vector $\mathbf{Y}^{\mathrm{pre}}$. In a similar manner, the rear vector $\mathbf{Y}^{\mathrm{post}}$, which has a length of L–2, is defined as:

$$\begin{aligned}\mathbf{Y}^{\mathrm{post}} &= \left[Y_0^{\mathrm{post}}[k_u],\, Y_1^{\mathrm{post}}[k_u], ..., Y_{L-2}^{\mathrm{post}}[k_u]\right] \\ &= Y_{L-1}[k_u] \times \left[Y_1[k_u],\, Y_2[k_u], ..., Y_{L-1}[k_u]\right],\end{aligned} \tag{9}$$

where $Y_l^{\mathrm{post}}[k_u]$ is the lth element of vector $\mathbf{Y}^{\mathrm{post}}$.

Finally, the extrapolated vector $\mathbf{Y}^{\mathrm{Ex}}[k_u]$ with of $2L-1$, is generated by concatenating $\mathbf{Y}^{\mathrm{pre}}$ and $\mathbf{Y}^{\mathrm{post}}$ as follows:

$$\mathbf{Y}^{\mathrm{Ex}} = \left[\mathbf{Y}^{\mathrm{pre}},\ \mathbf{Y}^{\mathrm{post}}\right]. \tag{10}$$

Since the signal length is extended from L to $2L-1$, an improvement in Doppler resolution is expected. As in the RoI-based algorithm where FFT is performed for Doppler estimation, an N_D-point FFT is applied to the extended signal. This allows the Doppler information of each target to be estimated.

4.2 Analysis of the Extrapolated Signals with Single Target

In this section, we mathematically analyze that the proposed extrapolation not only extends the length of the signal but also retains its sinusoidal characteristics. For simplification, considering a single target, the target index m is omitted, allowing a_m, τ_m, and f_m^{D} to be simplified as a, τ, and f^{D}, respectively. After RoI detection, (7) is simply expressed as follows:

$$Y_l[k_u] = A_{k_u} \exp\left(j2\pi f^D l T\right) + Z_l[k_u] \tag{12}$$

where A_{k_u} is the complex amplitude term after range FFT operation and $Z_l[k_u]$ is the k_u-th FFT output of $z_l[n]$. By substituting (12) into (8) and omitting noise $Z_l[k_u]$, the l-th element of $\mathbf{Y}^{\mathrm{pre}}$ are expressed as:

$$\begin{aligned}Y_l^{\mathrm{pre}}[k_u] &= Y_1[k_u]Y_l[k_u] \\ &= A_{k_u}^2 \exp\left(j2\pi\left(l+1\right)Tf^D\right) \ \text{ for } 0 \leqslant l \leqslant L-1.\end{aligned} \tag{13}$$

Similarly, the l-th element of $\mathbf{Y}^{\mathrm{post}}$ can be expressed as follows:

$$\begin{aligned}Y_l^{\mathrm{post}}[u] &= Y_{L-1}[u]Y_l[u] \\ &= A_{k_u}^2 \exp\left(j2\pi\left(L+l+1\right)Tf^D\right) \ \text{ for } 1 \leqslant l \leqslant L-1.\end{aligned} \tag{14}$$

By concatenating (13) and (14), we obtain (10), where the extended complex sinusoidal signal of length $2L-1$ is preserved.

To summarize the extrapolation procedure for a single target, Algorithm 1 presents a step-by-step construction of the extended signal based on vector multiplication and concatenation. This simple yet effective approach preserves the sinusoidal structure while doubling the signal length for improved Doppler resolution.

Algorithm 1 Extrapolated Signal Construction

Input: Original signal $\mathbf{y}[k_u] = [Y_0[k_u], Y_1[k_u], \ldots, Y_{L-1}[k_u]]$
Output: Extrapolated signal $\mathbf{y}^{\mathrm{Ex}}[k_u]$
/* Pre-part */
for $l = 0$ to $L-1$ **do**
  $Y_l^{\mathrm{pre}}[k_u] = Y_l[k_u] \cdot Y_1[k_u]$
end for
/* Post-part */
for $l = 1$ to $L-1$ **do**
  $Y_l^{\mathrm{post}}[k_u] = Y_{L-1}[k_u] \cdot Y_l[k_u]$
end for
Concatenate: $\mathbf{y}^{\mathrm{Ex}}[k_u] = [\mathbf{y}^{\mathrm{pre}}[k_u], \mathbf{y}^{\mathrm{post}}[k_u]]$

4.3 Analysis of the Extrapolated Signals with Multi-Target

In this section, we address the analysis of extrapolated signals in cases ranging from a single target to multiple targets. To simplify, the complex sinusoid signal due to Doppler frequency at the l-th chirp is denoted as ψ_m^l, i.e., $\psi_m^l = \exp\left(j2\pi T l f_m^D\right)$. Hence, $Y_l^{\mathrm{pre}}[k_u]$ is simply expressed as follows:

$$Y_l^{\mathrm{pre}}[k_u] = Y_1[k_u]Y_l[k_u] = \sum_{m=1}^{M} A_m\psi_m \sum_{m=1}^{M} A_m\psi_m^l \tag{15}$$

where A_m is the m-th target's complex amplitude term after range estimation. By expanding (15), the expression can be written in terms of a dot product term and a cross product term:

$$Y_l^{\mathrm{pre}}[k_u] = \underbrace{\sum_{m=1}^{M} A_m^2\psi_m^{l+1}}_{\text{dot product term}} + \underbrace{\sum_{m\neq p}^{M} A_m\psi_m \sum_{p\neq m}^{M} A_p\psi_p^l}_{\text{cross product term, } C^{\mathrm{pre}}}. \tag{16}$$

In the dot product term of (16), the sinusoidal structure is clearly preserved, as it contains Doppler information and exhibits a linear phase variation with respect to the index l. Meanwhile, the cross product term C^{pre} in (16) can be expanded as follows:

$$
\begin{aligned}
C^{\mathrm{pre}} &= A_1\psi_1\left(A_2\psi_2^l + A_3\psi_3^l + A_4\psi_4^l + \ldots\right) \\
&\quad + A_2\psi_2\left(A_1\psi_1^l + A_3\psi_3^l + A_4\psi_4^l + \ldots\right) \\
&\quad + \ldots + A_M\psi_M\left(A_1\psi_1^l + A_2\psi_2^l + A_3\psi_3^l + \ldots\right).
\end{aligned} \tag{17}
$$

By factoring out $A_m\psi_m^l$ from each product in (17), the expression can be rewritten as:

$$
\begin{aligned}
C^{\mathrm{pre}} &= A_1\psi_1^l\left(A_2\psi_2 + A_3\psi_3 + A_4\psi_4 + \ldots\right) \\
&\quad + A_2\psi_2^l\left(A_1\psi_1 + A_3\psi_3 + A_4\psi_4 + \ldots\right) \\
&\quad + \ldots + A_M\psi_M^l\left(A_1\psi_1 + A_2\psi_2 + A_3\psi_3 + \ldots\right).
\end{aligned} \tag{18}
$$

By expressing the terms inside the parentheses in (18) as $\tilde{A}_m$, i.e., $\tilde{A}_m = \sum_{m'\neq m}^{M} A_{m'}\psi_{m'}$, C^{pre}can be represented as another sinusoidal signal as follows:

$$
C^{\mathrm{pre}} = \sum_{m=1}^{M} \tilde{A}_m\psi_m^l. \tag{19}
$$

Similarly, by applying the same approach to the rear part, $Y_l^{\mathrm{post}}[k_u]$ is simply expressed as follows:

$$
\begin{aligned}
Y_l^{\mathrm{post}}[k_u] &= Y_{L-1}[k_u]Y_l[k_u] \\
&= \sum_{m=1}^{M} A_m\psi_m^{L-1} \sum_{m=1}^{M} A_m\psi_m^l \\
&= \underbrace{\sum_{m=1}^{M} A_m^2\psi_m^{L+l-1}}_{\text{dot product term}} + \underbrace{\sum_{m\neq p}^{M} A_m\psi_m^{L-1} \sum_{p\neq m}^{M} A_p\psi_p^l}_{\text{cross product term, } C^{\mathrm{post}}}
\end{aligned} \tag{20}
$$

where C^{post} is cross product term. As can be seen from (20), the dot product term in $Y_l^{\mathrm{post}}[k_u]$ is connected to the product term generated by $Y_l^{\mathrm{pre}}[k_u]$. Furthermore, the cross product component C^{post} can be analyzed as follows:

$$
\begin{aligned}
C^{\mathrm{post}} &= A_1\psi_1^{L-1}\left(A_2\psi_2^l + A_3\psi_3^l + \ldots\right) \\
&\quad + A_2\psi_2^{L-1}\left(A_1\psi_1^l + A_3\psi_3^l + \ldots\right) \\
&\quad + \ldots + A_M\psi_m^{L-1}\left(A_1\psi_1^l + A_2\psi_2^l + \ldots\right)
\end{aligned} \tag{21}
$$

By factoring out $A_m\psi_m^l$ from each product in (21), the expression can be rewritten as:

$$
\begin{aligned}
C^{\mathrm{post}} &= A_1\psi_1^l\left(A_2\psi_2^{L-1} + A_3\psi_3^{L-1} + \ldots\right) \\
&\quad + A_2\psi_2^l\left(A_1\psi_1^{L-1} + A_3\psi_3^{L-1} + \ldots\right) \\
&\quad + \ldots + A_M\psi_M^l\left(A_1\psi_1^{L-1} + A_2\psi_2^{L-1} + \ldots\right).
\end{aligned} \tag{22}
$$

By expressing the terms inside parentheses in (22) as $\hat{A}_m$, i.e., $\hat{A}_m = \sum_{m'\neq m}^{M} A_{m'}\psi_{m'}^{L-1}$, C^{post}can be represented as another sinusoidal signal as follows:

$$
C^{\mathrm{post}} = \sum_{m=1}^{M} \hat{A}_m\psi_m^l. \tag{23}
$$

As observed in (19) and (23), the dot product term becomes more dominant due to extrapolation, while the cross-product terms are composed of linear combinations of sinusoids sharing the same frequency components. Therefore, their overall influence on the frequency structure remains limited, and the extrapolated signal retains a strong sinusoidal behavior centered on the true Doppler frequency.

Moreover, while the extrapolation process operates on beat signals that include additive complex Gaussian noise, the operations involved—such as vector reversal, concatenation, and element-wise multiplication—introduce cross-terms involving noise products. Although these operations lead to non-Gaussian noise behavior, it is known that the product of independent complex Gaussian variables remains bounded with finite variance [16]. As a result, the extrapolated signal does not suffer from uncontrolled noise amplification. This robustness is supported by the simulation results in Sect. 5, where the proposed algorithm demonstrates superior resolution even under noisy conditions. Furthermore, the proposed algorithm assumes complex-valued input signals, as phase preservation is essential for extrapolation.

5 Performance Evaluation

5.1 Simulation Results

In this section, simulations are conducted to verify the resolution improvement of the proposed algorithm, and the results are reviewed. The conditions for the simulation are as follows: the center frequency f_c is 24 GHz, a chirp signal duration T is 400 μs, the bandwidth B is 500 MHz, the number of chirps per frame L is 40, the number of FFT points for range estimation N_R is 1024, and the number of FFT points for Doppler estimation N_D is 128.

Figure 9 compares the FFT input and output of the conventional FFT-based algorithm with the proposed algorithm for the single target with the velocity of 3 m/s. It can be observed that the signal length in the proposed algorithm is nearly twice as long as that in the conventional method. Additionally, the FFT output shows that the side-lobes of the proposed algorithm are smaller compared to those of the conventional FFT algorithm.

Figure 10 compares the FFT input and output of the conventional FFT-based algorithm with the proposed algorithm for two targets with the velocities of 3 m/s and 3.3 m/s. In Fig. 10(a), it can be observed that the signal length of the

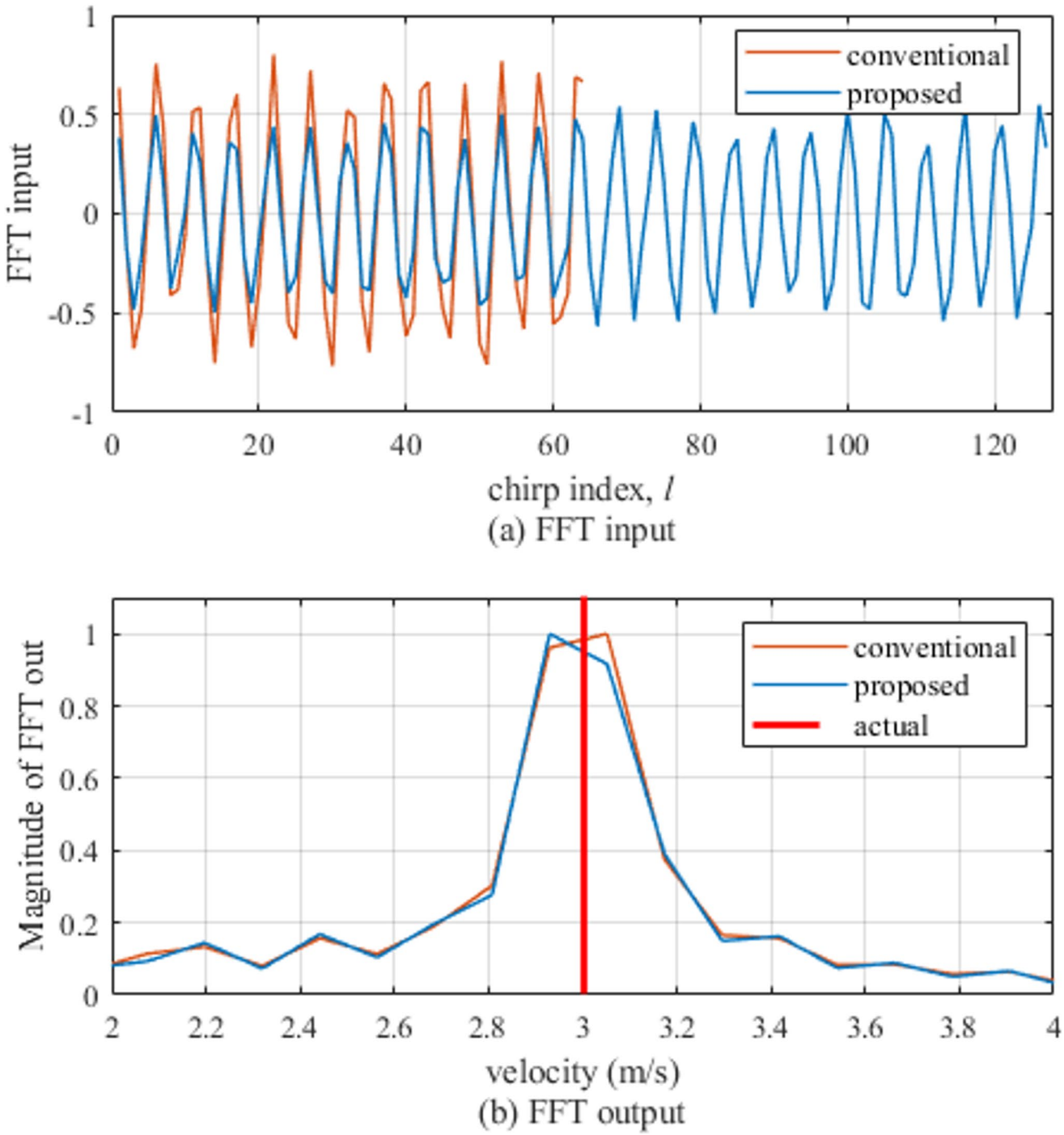

Fig. 9 Comparison of FFT input and output between the conventional and proposed algorithms with $M=1$

proposed algorithm is twice as long as that of the conventional algorithm. In Fig. 10(b), the conventional algorithm estimates a single target, whereas the proposed algorithm successfully estimates two targets.

Figure 11 illustrates the root mean square error (RMSE) of the estimated velocity difference between two targets under varying SNR conditions. RMSE is computed based on 10^4 independent simulation trials at each SNR. The three cases correspond to target velocities of v_1 = 5 m/s and v_2 = 5.2, 5.3, and 5.4 m/s, resulting in velocity differences of $\Delta v = 0.2$, 0.3, and 0.4 m/s, respectively. As expected, larger velocity separations lead to lower RMSE for all methods. The proposed algorithm outperforms the conventional FFT-based algorithm, particularly at lower SNRs and smaller

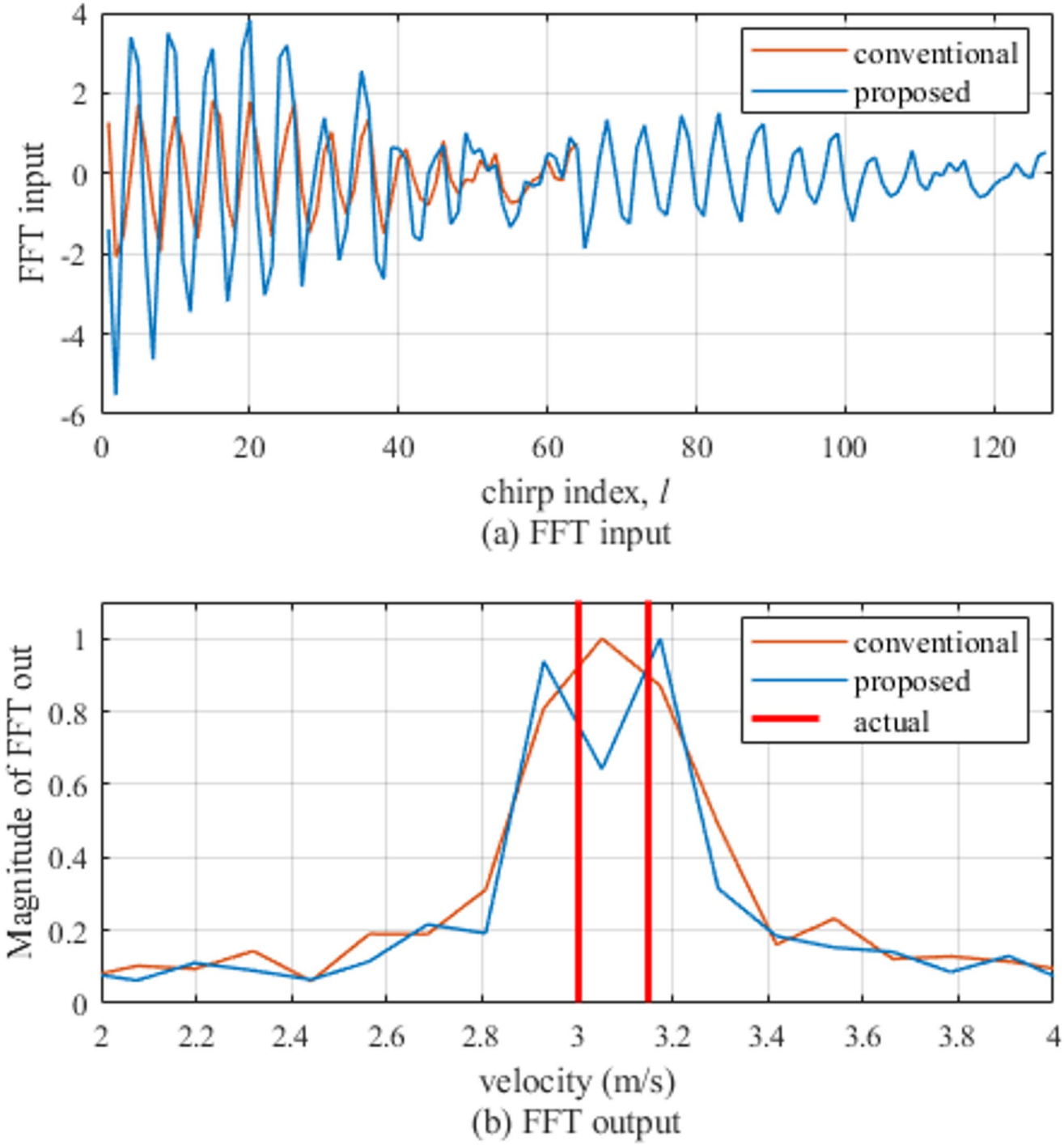

Fig. 10 Comparison of FFT input and output between the conventional and proposed algorithms with $M=2$

Δv. In contrast, the conventional algorithm shows relatively stable but inaccurate performance for small velocity differences due to its limited resolution. The MUSIC algorithm provides the best RMSE performance except at low SNRs, but this comes at the cost of significantly higher computational complexity. It is important to note that RMSE is computed only for detected targets. In cases where only a single peak is identified, the error is calculated based on the available estimate, while the missed target is excluded. Therefore, a low RMSE does not necessarily imply that both targets were successfully resolved, particularly for the conventional and MUSIC algorithms. This limitation is more clearly reflected in the missing rate results shown in Fig. 12.

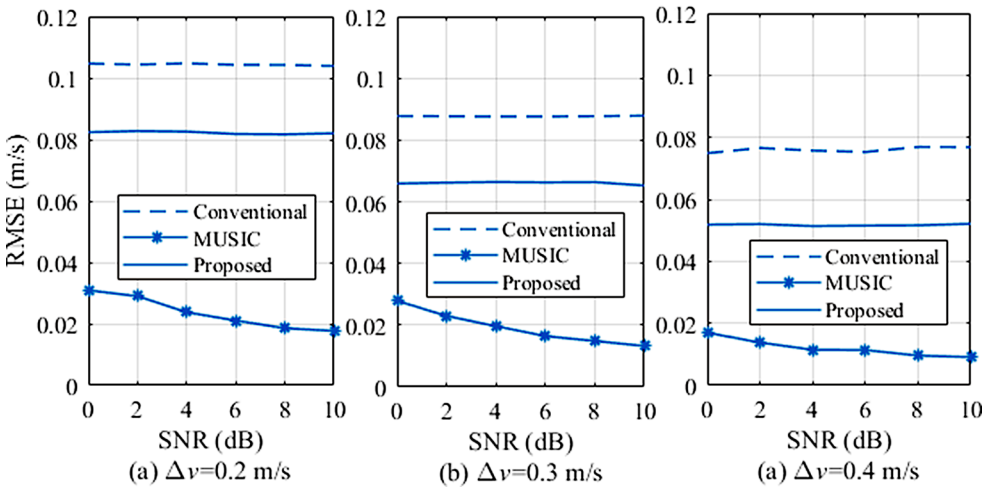

Fig. 11 RMSE of the estimated velocity with $M=2$

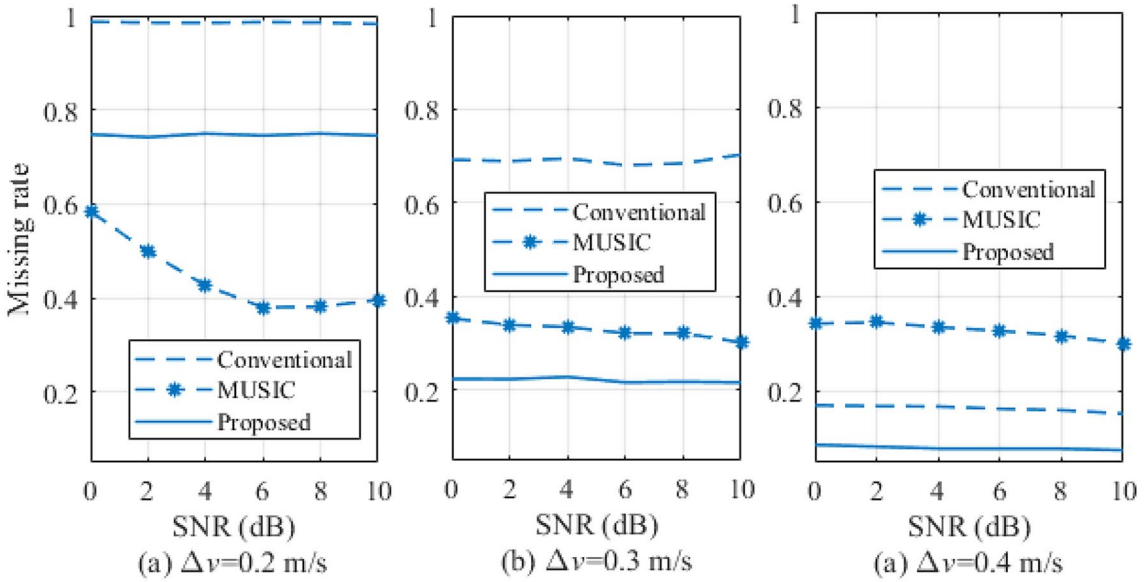

Fig. 12 Missing rate of the estimated velocity with $M=2$

Figure 12 shows the missing rate for each algorithm under the same conditions as in Fig. 11. The missing rate is defined as the proportion of trials in which both targets are not successfully detected either due to merging into a single peak or complete failure to detect one or both targets. Additionally, a trial is considered a miss if the estimation error exceeds 2 m/s. The proposed algorithm achieves a significantly lower missing rate than the conventional algorithm, particularly at smaller velocity differences, indicating superior robustness. In contrast, the conventional method exhibits a consistently high failure rate. Compared to the MUSIC algorithm, the proposed algorithm shows a higher missing rate when $\Delta v=0.2$ m/s, but achieves a lower missing rate for $\Delta v=0.3$ and 0.4 m/s. Despite its high resolution, MUSIC suffers from noise sensitivity, leading to higher missing rates than FFT-based methods under high SNR and sufficient target separation.

5.2 Complexity Analysis

This section analyzes the computational complexity of the conventional, the proposed, and the MUSIC algorithms. The comparison is based on the number of complex multiplications, which dominate the overall computation time in typical radar signal processing pipelines. To ensure a fair comparison, all methods are implemented with a RoI-based structure that limits Doppler estimation to N_p range bins identified as likely containing targets. Range estimation is commonly performed using an N_R-point FFT for all methods, providing the basis for subsequent Doppler processing.

For the RoI-based conventional algorithm, a total of $(1+L)\ N_R\ \log_2 N_R$ multiplications are required to perform one N_R-point FFT for RoI detection with high SNR, L additional N_R-point FFTs for range estimation processing across all chirps. Then, Doppler estimation is performed

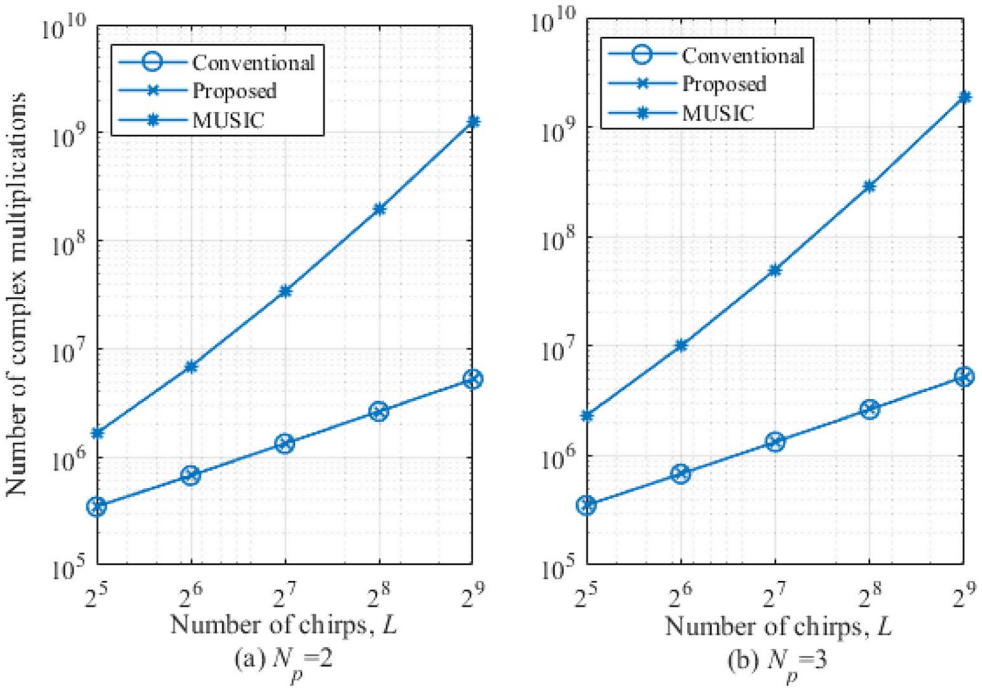

Fig. 13 Computational complexity comparison according to L

on N_p selected range bins using N_D-point FFTs, requiring $N_pN_D \log_2 N_D$ multiplications. Therefore, the total number of multiplications for the RoI-based conventional algorithm is given by:

$$C_{\text{conventional}} = (1+L)N_R\log_2 N_R + N_P N_D \log_2 N_D. \quad (24)$$

The proposed algorithm performs the same number of range FFTs, requiring $(1+L)\cdot N_R\log_2 N_R$ multiplications. After RoI detection, each of the N_p selected bins undergoes extrapolation, which involves simple signal operations equivalent to $2L$ multiplications per bin. Following extrapolation, Doppler estimation is performed using N_D-point FFTs for each extended signal. This step requires an additional N_p N_D $\log_2 N_D$ multiplications. Therefore, the total number of multiplications for the proposed algorithm is as follows:

$$C_{\text{proposed}} = (1+L)N_R\log_2 N_R + N_P(2L + N_D\log_2 N_D). \quad (25)$$

The MUSIC algorithm also begins with the same RoI detection and range processing stage, where an N_R-point FFT is applied to each of the L chirps, resulting in $LN_R\log_2 N_R$ complex multiplications. Based on the resulting range-Doppler map, N_p candidate range bins are selected as likely target locations. For each selected bin, Doppler estimation is performed using the MUSIC algorithm, where L chirps are treated as temporal snapshots to construct the sample covariance matrix. This includes covariance matrix estimation L^2, eigenvalue decomposition $16L^3/5$, projection matrix construction, and spectral evaluation over N_D points. These operations can be simplified and expressed as [17]:

$$C_{\text{MUSIC}} = (1+L)N_R\log_2 N_R + N_P L\left(\frac{16}{5}L^2 + \frac{(L-M)(L+1)}{2} + N_D(L+1)\right) \quad (26)$$

Table 1 Performance comparison of doppler Estimation algorithms

Algorithm	Resolution	Performance	Complexity
Conventional	~2.5 m/s	Low accuracy with high missing rate	Low
MUSIC	<0.5 m/s	High accuracy with high missing rate	Very high
Proposed	0.5~1 m/s	Moderate accuracy and low missing rate	Low

Figure 13 shows the computational complexity comparison in terms of the number of complex multiplications as a function of the number of chirps L. The proposed algorithm introduces moderate additional cost compared to the conventional approach, while the MUSIC algorithm requires significantly higher complexity, especially as L increases. As shown in Fig. 13, the proposed algorithm significantly reduces the number of complex multiplications compared to the MUSIC algorithm. For instance, when L=256 and N_p=2, the proposed algorithm requires approximately 240 times fewer complex multiplications than MUSIC. In the case of N_p=3, the gap remains substantial, with a reduction factor of about 360 times observed at L=512.

Table 1 summarizes the qualitative comparison among the conventional FFT-based method, the MUSIC algorithm, and

the proposed method in terms of Doppler resolution, estimation performance, and computational complexity. While the MUSIC algorithm provides the highest resolution, it suffers from a high missing rate and significantly increased complexity. The conventional FFT method is computationally efficient but exhibits low accuracy and high target miss rates. The proposed method offers a balanced trade-off, achieving moderate to high resolution and accuracy with low computational cost and reduced miss rates.

6 Conclusion

This paper proposed a Doppler resolution enhancement algorithm for FMCW radar that improves target separability without increasing observation time or computational complexity. By extrapolating the chirp signal through simple operations, the algorithm achieves higher Doppler resolution with minimal resource usage. Simulation results demonstrated superior performance in low SNR conditions, achieving lower missing rates and improved RMSE compared to conventional FFT-based methods, with similar computational cost. Future work includes validating the proposed method using real radar measurements. A 24 GHz FMCW radar system is being prepared to collect practical beat signals, and further studies will explore the algorithm's robustness in dynamic environments and potential integration with adaptive or AI-based techniques.

Acknowledgements This research was supported by the DGIST R&D Program of the Ministry of Science, ICT and Future Planning of Korea (25-IT-01), the Institute of Information & Communications Technology Planning & Evaluation (IITP) grant funded by the Korea government (MSIT) (No.2022-0-00521, Development of 5G-NR-V2X communication technology to support over Lv.4 autonomous driving service), and the 2025 academic research project of the Naval Institute for Ocean Research of the Republic of Korea Naval Academy.

Author Contributions Youngdoo Choi designed the core algorithm and drafted the manuscript. Seonghyun Jang conducted the simulations. Bong-seok Kim designed and developed the core algorithm, conducted the simulations, analyzed the results, and reviewed the manuscript. Sangdong Kim supervised the overall research direction and contributed to manuscript revisions. All authors read and approved the final manuscript.

Funding Open Access funding enabled and organized by DGIST (Daegu Gyeongbuk Institute of Science & Technology)

Data Availability The datasets generated during the current study are not publicly available as the results are based on simulations that can be independently reproduced, and institutional policy restricts data sharing.

Declarations

Competing Interests Youngdoo Choi, Seonghyun Jang, Bong-seok Kim, and Sangdong Kim declare that we have no competing financial interests or personal relationships that could have appeared to influence the work reported in this paper.

References

1. Skolnik MI (2001) Introduction to radar systems, 3rd edn. McGraw-Hill, New York, USA
2. Richards MA, Scheer JA, Holm WA (2010) Principles of modern radar: Basic principles. SciTech Publishing, Raleigh, USA
3. Rohling H, Mende M (2008) A fast FMCW radar signal processing algorithm for high accuracy measurements. In Proceedings of the IEEE Radar Conference, Rome, Italy, 1–4
4. Hasch J et al (Mar. 2012) Millimeter-wave technology for automotive radar sensors in the 77 GHz frequency band. IEEE Trans. Microwave Theory Techn 60(3):845–860
5. Almasri MO, Hindia MN, Azizan MA, Ali MAM, Reza AW (Jun. 2022) Low-complexity direction-of-arrival estimation using FFT-based beamspace root-MUSIC. IEEE Sensors J 22(11):10239–10246
6. Ye H, Dai Y, Zheng H, Jia Z, Liang D, Tang J (Oct. 2024) An efficient conflict-free 2-D FFT for FMCW radar imaging on DSP. IEEE Trans Instrum Meas 73:Art.8508711
7. Singh TH, Huang P-T, Kao K-S, Cheng C-S, Wen K-A, Wang L-C (Apr. 2024) Energy-efficient sparse FFT and compressed transpose memory for MmWave FMCW radar sensor system. IEEE Trans Instrum Meas 73:Art.8503611
8. Kim B, Kim S, Lee J (May. 2018) A novel DFT-based DOA estimation by a virtual array extension using simple multiplications for FMCW radar. Sensors 18(5):1560
9. Neemat S, Uysal F, Krasnov O, Yarovoy A (Oct. 2019) Reconfigurable range-Doppler processing and range resolution improvement for FMCW radar. IEEE Sens J 19(20):9294–9303
10. Roy R, Kailath T (Jul 1989) ESPRIT—Estimation of signal parameters via rotational invariance techniques. IEEE Trans Acoust Speech Signal Process 37(7):984–995
11. Li Y-C, Choi B, Chong J-W, Oh D (May. 2018) 3D target localization of modified 3D MUSIC for a triple-channel K-band radar. Sensors 18(5):1634
12. Nam H, Li Y-C, Choi B, Oh D (Apr. 2018) 3D-subspace-based auto-paired azimuth angle, elevation angle, and range estimation for 24G FMCW radar with an L-shaped array. Sensors 18(4):1113
13. Schmidt RO (Mar. 1986) Multiple emitter location and signal parameter estimation. IEEE Trans Antennas Propag 34(3):276–280
14. Kim B, Kim S, Lee J (Jan. 2020) Low-complexity joint range and Doppler FMCW radar algorithm based on number of targets. Sensors 20(1):51

15. Kim S, Kim B, Choi Y (2024) Doppler resolution improvement algorithm for radar systems. Mar Sci Technol 18:1–15
16. Bromiley PA (2003) Products and convolutions of gaussian probability density functions, TINA Technical Memo 2003-003, Univ. of Manchester
17. Baig NA, Malik MB (Dec. 2013) Comparison of direction of arrival (DOA) estimation techniques for closely spaced targets. Int J Future Comput Commun 2(6):654–659

Yongdoo Choi He obtained a Bachelor's degree in Oceanography from the Korea Naval Academy, a Master's degree in Electrical, Electronic and Computer Engineering from Kyungpook National University, and a Ph.D. in Electronic Engineering from the same university. During his doctoral studies, he specialized in underwater acoustic signal processing. He is currently serving as a professor of Electrical and Electronic Engineering at the Korea Naval Academy. His main research areas include underwater target detection, unmanned surface vehicle (USV) operation, and manned-unmanned teaming (MUM-T) systems. He has participated in projects such as the combat system AI development project for Hanwha Systems.

Seonghyun Jang He received B.S degree in electronic and computer engineering from Hanyang University, Seoul, South Korea, in 2006, and the Ph.D. degree in electronic and computer engineering from the same university in 2013. From 2013 to 2021, he was a Principal Research Engineer with the Modem Development Team, System LSI Division, Samsung Electronics, Hwaseong, South Korea. Since 2021, he has been a Principal Researcher with the Mobility Platform Research Center, Korea Electronics Technology Institute, Seongnam, South Korea. His current research interests include communication systems and radar signal processing.

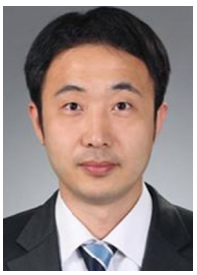

Bong-seok Kim He received the B.S. degree in electronics engineering from Yeungnam University, Gyeongsan, South Korea, in 2006, and the M.S. and Ph.D. degrees in information and communications engineering from Yeungnam University, in 2009 and 2014,respectively. Since 2016, he has been a Senior Research Engineer with Daegu Gyeongbuk Institute of Science and Technology (DGIST), Daegu, South Korea. His current research interests include multifunctional radar systems and radar signal processing.

Sangdong Kim He received a B.S. degree from Hanyang University in 2004, a M.S. degree from Hanyang University in 2006, and a Ph.D. from Kyungpook National University in 2018, all in electronics engineering. Since 2006, he has been a Principal Researcher and a Concurrent Associate Professor with DGIST, South Korea. From 2015 to 2016, he was a Visiting Scholar with the University of Florida, Gainesville, FL, USA. From 2022 to 2023, he was a Visiting Scholar with The Pennsylvania State University, University Park, PA, USA. His research interests include super-resolution algorithms, automotive radar, vital sign radar, and 3D lidar object detection.